Available online at www.sciencedirect.com
ScienceDirect
Earth and Planetary Science Letters 261 (2007) 565–577
EPSL
www.elsevier.com/locate/epsl

Sinking hot anomaly trapped at the 410 km discontinuity near the Honshu subduction zone, Japan

Satoru Honda *, Manabu Morishige, Yuji Orihashi

Earthquake Research Institute, University of Tokyo, 1-1-1, Yayoi, Bunkyo-ku, Tokyo 113-0032, Japan

Received 7 October 2006; received in revised form 17 May 2007; accepted 12 July 2007
Available online 24 July 2007
Editor: C.P. Jaupart

Abstract

A fate of hot anomaly dragged down by subducting slab is studied by simple 2D and 3D fluid dynamical models in which the slab movement is kinematically imposed. The 410 km discontinuity, treated as an olivine–wadsleyite phase change, acts as a barrier to the downward movement of hot anomaly. As a result, the hottest part is located near the 410 km discontinuity. The shape of high temperature anomaly near the 410 km discontinuity is similar to that of the low velocity anomaly under the ocean-ward side of the subduction zone near the Honshu arc, Japan, which was recently convincingly confirmed, and it was interpreted as a mainly thermal anomaly. The time for the hot anomaly to stay near the 410 km discontinuity depends on many factors, such as the intensity of thermal anomalies and the viscosity. We set up a simple model in which such a hot anomaly was produced in the area of the Pacific superplume region and carried toward the Japanese Islands by the horizontal flow associated with the plate movement. The hot anomaly whose size is equivalent to 2–3000 km (horizontal) × 200 km (vertical) may stay there longer than ~100 million yr. We will discuss the implication of this result in terms of the relation between the present high temperature anomaly near the Honshu subduction zone and the past activity of the Pacific superplume.

Keywords: 410 km discontinuity; seismic tomography; superplume

1. Introduction

The Earth's mantle contains a several phase changes and their effects on the mantle flow has long been discussed (e.g., Christensen and Yuen, 1985; Honda et al., 1993; Tackley et al., 1993; Zhong and Gurnis, 1994; van Hunen et al., 2001). Especially, the interaction between the sinking cold slab and the endothermic phase change, which is supposed to be the origin of 670 km seismic discontinuity, is found to be interesting because of its hindering nature toward the mantle flow. The shallower exothermic phase change near the 410 km seismic discontinuity is believed to promote the movement of sinking slab and rising hot plume (e.g., Schubert et al., 1975).

Tomographic results provide important insight into the structure of the Earth's interior. For example, the fast velocity anomaly observed near the 670 km boundary

* Corresponding author. Tel.: +81 3 5841 5725; fax: +81 3 5802 3391.
E-mail addresses: honda@eri.u-tokyo.ac.jp (S. Honda), stellvia@eri.u-tokyo.ac.jp (M. Morishige), oripachi@eri.u-tokyo.ac.jp (Y. Orihashi).

0012-821X/$ - see front matter © 2007 Elsevier B.V. All rights reserved.
doi:10.1016/j.epsl.2007.07.028

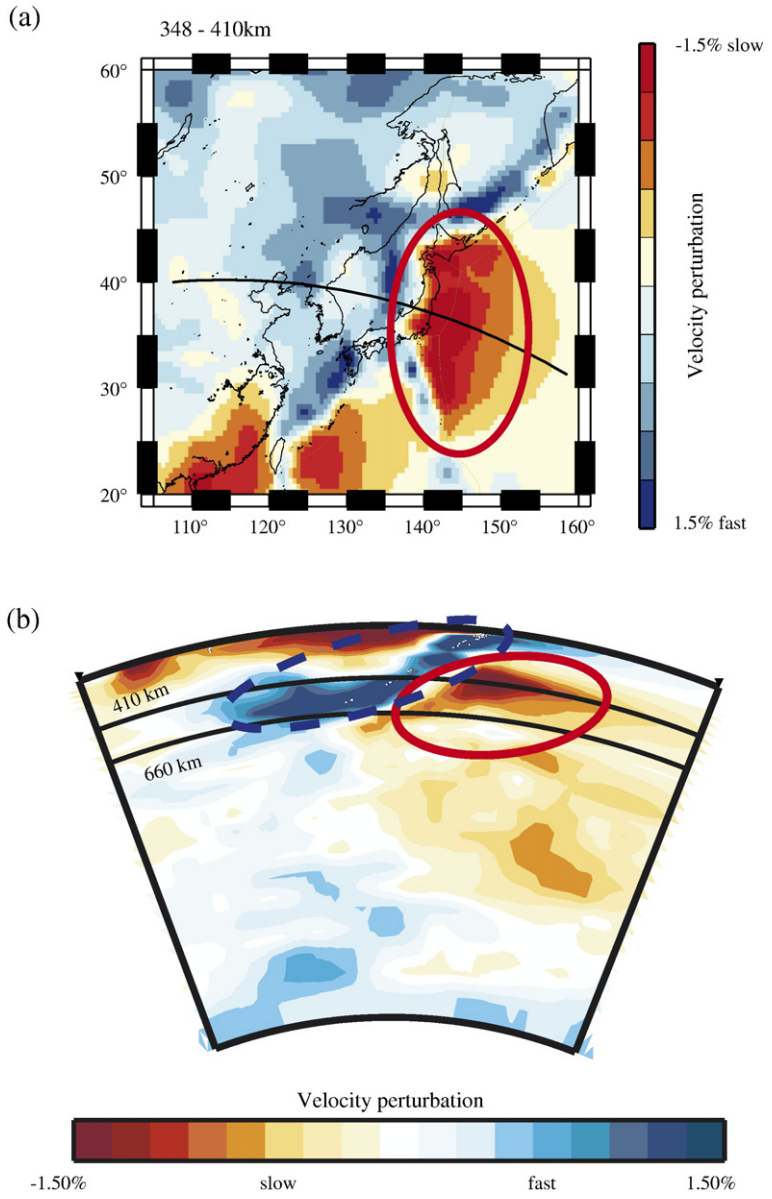

Fig. 1. Tomographic results around Japan (Obayashi et al., 2006). Figures (a) and (b) show, respectively, the horizontal cross section at 348–410 km depth and the vertical cross section along the great circle shown in (a). Solid ellipses show the position of low velocity zone which we are discussing. Dashed ellipse shows the position of high velocity zone supposedly related to the subduction of the Pacific plate.

(e.g. Fukao et al., 2001) may be an evidence of hindering nature of the endothermic phase change toward the movement of the subducting cold slabs. Recently, Obayashi et al. (2006) studied the slow seismic velocity anomaly beneath the ocean-ward side of the Japanese subduction zone (Fig. 1). The existence of the slow velocity anomaly adjacent to the fast velocity anomaly itself is not surprising, because it is a natural consequence of the definition of the anomalies, that is, the deviations from the average structure. Actually, one may see such features near the fast velocity anomalies associated with subducting slabs in the previously published tomographic results.

Although we cannot evaluate the quality of tomographic results, we have done a simple visual check of low velocity anomaly, whose distribution is similar to that of Fig. 1 in the previously published tomographic results (Obayashi et al., 1997; van der Hilst et al., 1997; Widiyantoro, 1997; Zhao et al., 1997; Kárason and van der Hilst, 2000; Piomallo and Moreili, 2003; Miller

Table 1
Visual check of low velocity anomalies under the subducting slabs

Subduction zone[1)]	WEPP2[2)]	P97[3)]	W[4)]	KV[5)]	PM[6)]	Zetal[7)]	MKG[8)]
Aleutian		Δ	?				
South Kurile	Δ	O					
Japan	O	O		O			Δ
Izu-Bonin	O	O					
Java	×	O		Δ			
Tonga		O	O	O		×	
South America		Δ	O				
Central America		?	?	O			
Aegean				O	?		

[1)]The subduction zones roughly correspond to those of Fukao et al. (2001). [2)]Obayashi et al. (1997). See Fukao et al. (2001). [3)]van der Hilst et al. (1997). See Fukao et al. (2001). [4)]Widiyantoro (1997). See Fukao et al. (2001). [5)]Kárason and van der Hilst (2000). [6)]Piomallo and Moreili (2003). [7)]Zhao et al. (1997). [8)]Miller et al. (2006).

et al., 2006). The results are summarized in Table 1. Note that we have no intention to give any concrete statements. Instead, we try to stress the importance of those features in geodynamics. In Table 1, the circles, the triangles and crosses imply that the low velocity zone is visible, that it is vaguely visible and that it is not visible, respectively. Question marks imply that the low velocity is visible but its interpretation is difficult. In the Aleutian and the Central America subduction zones, the slab is not clearly visible and/or the low velocity anomaly might be a continuation of regional low velocity anomalies under the ocean-ward side of the subduction zone. In the Aegean subduction zone, the global model of K´arason and van der Hilst (2000) shows its existence. However, the regional study done by Piomallo and Moreili (2003) shows that such a low velocity anomaly appears to exist ubiquitously even outside the subduction zone. Thus, we judged that its origin is somewhat questionable. In the Tonga subduction zone, we see the low velocity zone in globally based models, but the regional model presented by Zhao et al. (1997) does not show such a feature (or very vague feature).

As shown above, we still have lots of ambiguities in the interpretation of tomographic results. Thus, the main issue here is the solid confirmation of its existence, determination of its distribution and magnitude. Based on the seismological arguments, Obayashi et al. (2006) firstly confirmed the existence of a hot thermal anomaly near the Honshu subduction zone and concluded that it is mainly thermal anomaly whose magnitude is ≈200 °C. They interpreted it as a hot plume rising near the Honshu subduction zone. However, from a close look at the seismic anomaly, we notice that the slow velocity anomalies are fairly well-correlated with the 410 km discontinuity. This appears to contradict the above-mentioned notion that the phase change related to the 410 km discontinuity acts as a driving agency of the rising hot anomaly. If the phase change drives the flow, the hot anomaly should leave it quickly.

Consider a situation that a hot anomaly, which may be the remnant of past plume head or stem, happens to be carried by the plate movement toward the subduction zone and eventually sinks down because of the mantle flow caused by the sinking slab. If the hot anomaly sinks down, the role of the 410 km discontinuity will be to prevent the “downgoing” movement of hot anomaly. Thus, we may expect a feature similar to the one found by Obayashi et al. (2006). In addition to this interest on the distribution of hot anomaly, we are also interested in its origin, that is, how it was created and where it came from. In this paper, we try to answer these questions using simple 2D and 3D numerical flow models.

We will consider a simple scenario in which the hot anomaly came from the possible past active upwelling region in the Pacific, that is, a superplume (Larson, 1991a,b). This scenario is similar to that of VanDecar et al. (1995) who found the low velocity anomalies occupying the whole upper mantle beneath Brazil. They attributed its origin to the fossil plume whose activity was related to the breakup of Gondowanaland at ~145 Ma.

In Japanese Islands, several researchers (Kimura et al., 1994; Maruyama et al., 1997; Tatsumi et al., 1998;

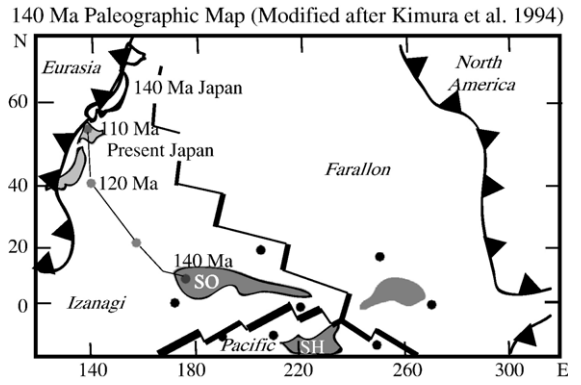

Fig. 2. Paleogeographic map of the Pacific Ocean in 140 Ma modified after Kimura et al. (1994). Black dots are the present locations of hot spots. Thin lines show the trajectory of Sorachi plateau. Locations of present and past (140 Ma) Japanese Islands are shown by gray area and closed curves, respectively. The meaning of symbols are: SO: Sorachi plateau, SH: Shatzky Rise.

Terabayashi et al., 2005) inferred that the seamounts and/or oceanic plateau concerned with the superplume activities (Larson, 1991a,b) might have subducted in the Cretaceous ages. Their arguments are based on the petrological/geochemical identification of plume material in the terrains and the reconstruction of past plate movement. The plume-like materials are identified in Sorachi-Yezo belt in Hokkaido (northern part of Japan) (Kimura et al., 1994) and in Sambagawa and Mikabu belts in Shikoku (western part of Japan) (Maruyama et al., 1997; Tatsumi et al., 1998; Terabayashi et al., 2005). Ueda (2005) concluded that the Kamuikotan zone in the Sorachi-Yezo belt was formed by the accretion of seamounts which might also be a superplume origin. Their formation ages are older than the age when the presently extinct Izanagi plate (Farrar and Dixon, 1981) was subducting beneath the Japanese Island. Kimura et al. (1994) presented clearer view of this scenario to explain the past history of Sorachi oceanic plateau and we construct a model setting based on his scenario (see below). We also note that Larson (1991b) presumed that the half of the plateaus formed at ~80 Ma superplume might have subducted beneath the continental margin of South America. However, as far as we know, no comparable petrologic/geochemical studies to those mentioned above on this subject have been reported yet.

2. Model

Fig. 2 summarizes the geologic observations and inferences related to the accretion of superplume-

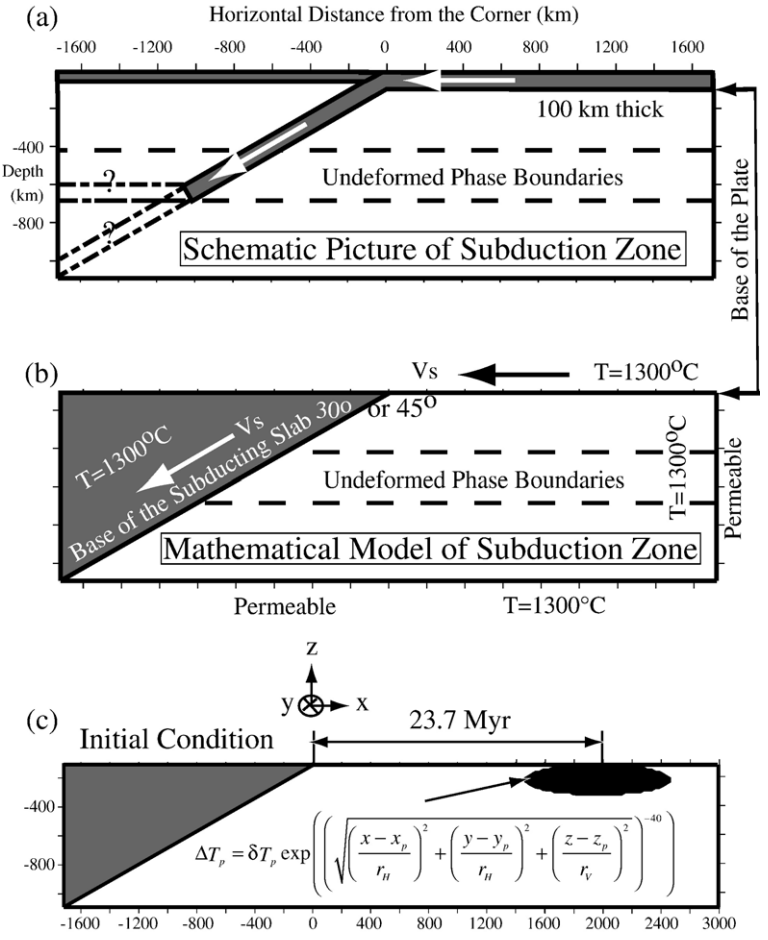

Fig. 3. Schematic picture (a), mathematical model (b) and the initial condition (c) of subduction zone model. The gray areas show the overlying lithosphere and subducting lithosphere which may or may not stagnate. In mathematical model, we only consider the wedge mantle of the ocean-ward side of the subduction zone. Dashed lines are the positions of phase changes at T=1300 °C. Black region in (c) represents the temperature anomaly. See the text for other details.

related rocks to the Japanese Islands by Kimura et al. (1994).

They studied the accreted oceanic plateau (Sorachi plateau) in Hokkaido area and identified the plume material. They also showed the trajectory of accreted plateau based on the paleo-reconstruction of plate movement and found that its birthplace was located in the South Pacific (Fig. 2). Based on this result, we assume that the plume material reached the Japanese Islands 23.7 Myr (~25 Myr) after the formation of the upwelling in our modeling.

Fig. 3 shows a schematic view of a subduction zone (a) and corresponding our mathematical model (b) and initial condition (c). Subducting and over-lying lithospheres are shown by gray area. Most of our computational models are two-dimensional. A several 3D models are used to evaluate the 3D effects on the results. The 3D model extends to the direction normal to Fig. 3. The model only takes into account the wedge mantle of the ocean-ward side of the subduction zone. The thickness of the overlying lithosphere is assumed to be 100 km, that is, only the mantle below 100 km depth is considered. The speed of the plate movement V_s is imposed both on the top surface and subducting slab (gray area in Fig. 3b and c). The temperature surrounding the area is set to a background temperature (Tm = 1300 °C), so that we mainly consider the mechanical influence of the moving lithosphere. We may underestimate the heat sink effects of subducting and overlying lithospheres. However, note that the constant temperature on the top surface and the subducting slab still acts as a heat sink, because the temperature of hot anomaly is higher than the background mantle temperature of 1300 °C. Flow boundary conditions at side and bottom boundaries are permeable, that is, the velocity gradient normal to the boundaries and the velocity parallel to the boundaries are set to zero. For 3D models, we assume impermeable, free-slip and reflective in temperature at side walls.

Fig. 3c shows an initial condition of temperature field. We define the corner of the mantle as the origin of the horizontal axes (Fig. 3c). For vertical direction the origin is taken at the surface. We impose the temperature anomaly ΔT_p given by,

$$\Delta T_p = \delta T_p \exp\left(\left(\sqrt{((x-x_p)/r_H)^2 + ((y-y_p)/r_H)^2 + ((z-z_p)/r_V)^2}\right)^{-40}\right) \quad (1)$$

which is similar to that of Cordery et al. (1997). δT_p is the temperature anomaly at x (horizontal distance) $= x_p$, y (horizontal distance) $= y_p$ and z (vertical distance, i.e., depth) $= z_p$ (= −200 km: fixed), that is, the center of initial temperature anomaly. r_H and r_V (= 100 km: fixed) characterize the shape of temperature anomaly. For two dimensional models, we simply drop the term related to y. Note that the plan view of the thermal anomaly for 3D cases is circular.

As discussed above, the position of the center of the anomaly is set so that the distance between the center of the plume and the corner of the mantle is $V_s \times 23.7$ (Myr). If we consider the fairly complicated plate movement during the past 100–200 Ma (Maruyama et al., 1997), our model is a bold simplification. However, from ~100 Ma, only the Pacific plate with the speed of ~9 cm/yr was subducting near the Japanese Islands (Maruyama et al., 1997) which may partially warrant our simplification.

Assuming the existence of giant upwelling in the past, it is difficult to estimate how large the past upwelling was. Larson (1991a) estimated its minimum size is about 6000 × 10,000 km based on the paleo-

Table 2
Parameters used in this study

Symbol	Value
g (gravity)	(10) m/s^2
α (volume thermal expansivity)	(3×10^{-5}) 1/K
Tm (unperturbed mantle temperature)	(1300) °C
d (depth)	(10^6) m
ρ_0 (reference density)	(4000) kg/m^3
η_{ref} (viscosity at Tm)	(5×10^{20}) [a], 2.5×10^{20} Pa s
κ (thermal diffusion coefficient)	(10^{-6}) m/s^2
E (activation energy)	(0), 153, 255 kJ/mol
$\delta\rho_1$ (density jump at 410 km)	$\delta\rho_1/\rho$ = (9)% [b], 6%
$\delta\rho_2$ (density jump at 670 km)	$\delta\rho_2/\rho$ = (9)% [b]
$\delta\rho_3$ (density jump at 500 km)	$\delta\rho_3/\rho$ = 3%
γ_1 (Clapeyron slope)	(3.7) [c], 2.5 MPa/K
γ_2 (Clapeyron slope)	(−2.8) [d] MPa/K
γ_3 (Clapeyron slope)	6.9 [c] MPa/K
$Tp_1 = Tp_2 = Tp_3$ [e]	(1300) °C
dp_1 [e]	(410) km
dp_2 [e]	(670) km
dp_3 [e]	500 km
$wp_1 = wp_2 = wp_3$ [e]	(10) km
δT_p [e]	(260), 300, 325 °C
x_p [e]	km
y_p [e]	km
z_p [e]	(200) km
r_H [e]	(500), 1000, 1500 km
r_V [e]	(100) km
V_s (speed of subduction)	(10), 5 cm/yr

[a] Lambeck and Johnston (1998).
[b] Christensen (1996).
[c] Katsura et al. (2004).
[d] Hirose (2002).
[e] See text.

Table 3
Parameters used for the models shown in the figures

Figure no.	4a	4b	6[a)]	7a	7b[b)]	7c[c)]	7d	9a	9b	9c	9d
η_{ref}[1)]	5	5	5	2.5	2.5	2.5	2.5	5	5	5	5
E[2)]	0	0	0	0	0	0	0	0	255	255	133
$\delta\rho_1$[3)]	9	–	9	9	9	9	6	9	9	6	6
$\delta\rho_3$[3)]	–	–	–	–	–	–	3	–	–	3	3
γ_1[4)]	3.7	–	3.7	3.7	3.7	3.7	2.5	3.7	3.7	2.5	2.5
γ_3[4)]	–	–	–	–	–	–	6.9	–	–	6.9	6.9
dp_3[5)]	–	–	–	–	–	–	500	–	–	500	500
δT_p[6)]	260	260	260	300	300	300	300	325	325	325	325
r_H[7)]	500	500	1000	1500	1500	1500	1500	1500	1500	1500	1500
V_s[8)]	10	10	10	10	10	10	10	10	10	10	10
H[9)]	5196	5196	5413×2706	5954	5954	5000	5954	5954	5954	5954	5954
T_R[10)]	52.6	44.4	65.5	151	151	128	146	123	142	177	157

[1)]$\times 10^{20}$ Pa s. [2)]kJ/mol. [3)]%. [4)]MPa/K. [5)]km. [6)]°C. [7)]km. [8]cm/yr. [9)]Horizontal distance (km). [10)]Residence time in Myr. [a)]3D case. [b)]Same as 7a with double resolution. [c)]Same as 7a with 45° dip angle.

reconstruction of the distribution of oceanic plateau. Assuming a part of such an upwelling reached the Japanese Islands, the upper limit of diameter $2r_H$ may be around ~3000 km. This single plume-head like thermal anomaly does not mean the existence of such a plume. It may be an equivalent size of number of plumes (Schubert et al., 2004).

As commonly assumed, the mantle is treated as an incompressible, Boussinesq Newtonian viscous fluid in which the inertia terms of the equations of motion are neglected. The basic equations for this medium are given by

$$\nabla \cdot \underline{v} = 0 \tag{2}$$

$$\nabla \cdot \underline{\underline{\tau}} - \nabla p = \rho g \underline{\hat{z}} \tag{3}$$

$$\tau_{ij} = \eta(v_{i,j} + v_{j,i}) \tag{4}$$

$$\frac{\partial T}{\partial t} + \underline{v} \cdot \nabla T = \kappa \nabla^2 T \tag{5}$$

where $\underline{v}$ is the velocity, $\underline{\underline{\tau}}(\tau_{i,j} : (i,j,k) = (x,y,z))$ is the stress tensor, p is the pressure, ρ is the density, g is the gravity, η is the viscosity, T is the temperature in Celsius degree, $\underline{\hat{z}}$ is the unit vertical vector (positive upward), t is the time and κ is the thermal diffusivity. The density change $\delta\rho_{ph}$ associated with the phase changes is added to the density variation of thermal origin as,

$$\rho = \rho_0(1 - \alpha T) + \delta\rho_{ph} \tag{6}$$

where ρ_0 is the reference density and α is the coefficient of thermal expansion. $\delta\rho_{ph}$ may be given by (e.g., Christensen and Yuen, 1985).

$$\delta\rho_{ph} = \sum_i \delta\rho_i \Gamma(\pi_i / wp_i) \tag{7}$$

$$\Gamma(\pi_i / wp_i) = (1 + \tanh(\pi_i / wp_i))/2 \tag{8}$$

$$\pi_i = d - dp_i - \gamma_i/(\rho_0 g)(T - Tpi) \tag{9}$$

where $\delta\rho_i$ is the density change of i-th phase change (i=1: olivine–wadsleyite phase change at 410 km; i=2: endothermic phase change at 670 km) and the phase change occurs at the depth dp_i with temperature of Tpi. wp_i characterizes the sharpness of the phase boundary. d is the depth. Later, we will introduce another phase boundary which may be related to the wadsleyite–ringwoodite phase change.

For most cases, the viscosity is assumed to be temperature-independent mainly for the ease of calculation and interpretation. We assume the viscosity jump of factor 30 below the 670 km phase boundary (Hager, 1984). We also consider a several cases in which the viscosity follows Arrhenius type of law without the pressure dependence as

$$\eta = \eta_0 \exp(E/R/(T + 273.15)) \tag{10}$$

where E and R are the activation energy and universal gas constant, respectively. The constant η_0 is set to the value so that the viscosity at 1300 °C becomes η_{ref} (reference viscosity; see Tables 2 and 3).

The basic equations describing the conservation of mass, linear momentum and energy coupled with constitutive equations and the equation of state are discretized using the finite volumes. For our purpose, the code developed by Tackley (1993) (i.e. 'stag3d') was

modified to incorporate the kinematically moving slab. The aspect ratio (depth : horizontal distance) of the finite volumes is $1 : \sqrt{3}$ and the depth of the layer is 1000 km. However, for one case, we use the rectangular finite volumes to check the effects of the different dip angle (=45°). The total horizontal length of model is variable in order to reserve the space for the distance between the corner of the mantle and the position of the anomaly, and anomaly itself. For most cases, dip angle and V_s are set, respectively, to 30° and 10 cm/yr, except for a several cases, to mimic the Honshu subduction zone, Japan. Most cases use 64 finite volumes for vertical and several cases use 128 finite volumes to check the accuracy.

The parameters used in this study are summarized in Table 2.

We define the reference model whose parameters are shown with brackets in Table 2. In Table 3, we list the variable parameters used and the output of the models shown in the figures.

3. Results

3.1. Constant viscosity cases

Fig. 4 shows the cases with ((a): reference case), and without olivine–wadsleyite phase change (b). The numerals in Fig. 4 indicate the time elapsed after the start of simulation. From these figures, it is clear that the hot anomaly is trapped at the 410 km discontinuity for a while, if the model includes the olivine–wadsleyite phase change. It is noteworthy that the highest temperature anomaly is located above the 410 km phase boundary. This behavior can be observed in any shape of hot anomaly, but the duration in which the hot anomaly is trapped (We call this "residence time", hereafter) depends on various parameters. Thus, we shall look at the effects of various parameters on the residence time below.

We examined the effects of V_s, η_{ref} , δT_p and three dimensionality on the residence time. As described before, the highest temperature for the cases with olivine–wadsleyite phase change is located above 410 km. Thus, we monitored the evolution of the maximum temperature with time. Then, we define the residence time as the time during which the maximum temperature is above 1500 °C (i.e., 200 °C higher than the background temperature). The results are summarized in Fig. 5 in which the ordinate and abscissa are the residence time and the approximate diameter of hot anomaly (i.e., $2r_H$), respectively.

By comparing the results of 2D cases ("Reference 2D" in Fig. 5) and corresponding 3D cases ("Reference 3D"), we found that the residence times of three-dimensional cases are 64% (r_H=500 km), 68% (r_H=700 km) and 75% (r_H=1000 km) of corresponding two-dimensional cases. Based on these results, we show estimated two-dimensional equivalent times of 100 Myr

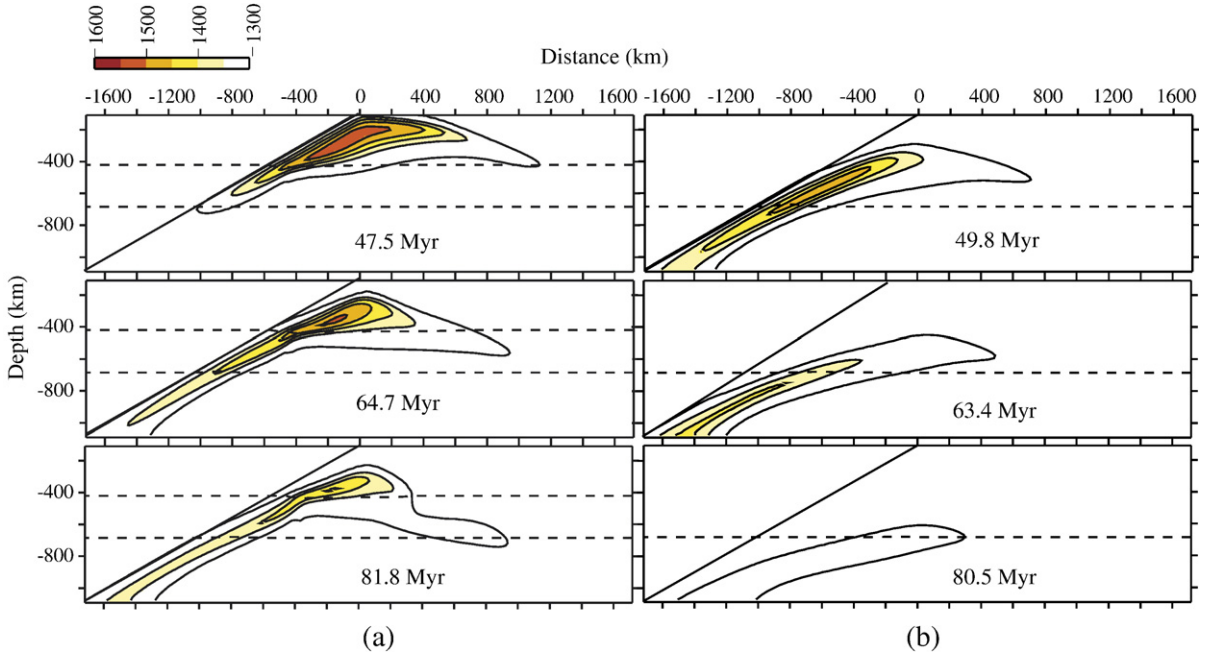

Fig. 4. Results (temperature) of with ((a): reference case) and without (b) olivine–wadsleyite phase change. Numerals show the time elapsed after the start of calculations.

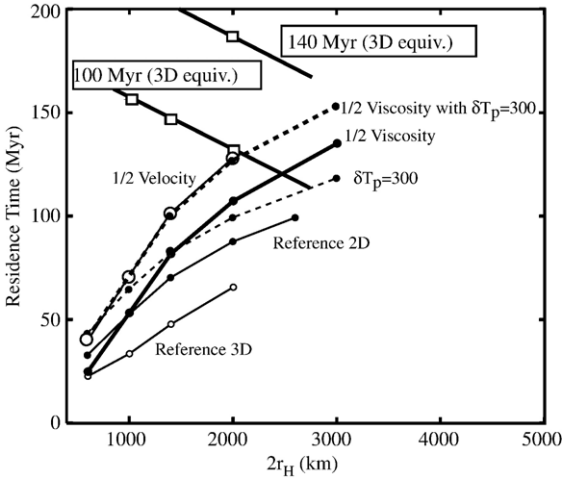

Fig. 5. Relationship between the horizontal diameter of thermal anomaly ($2r_H$) and the residence time. Various lines connect the cases with the same parameters except r_H. Thick lines with rectangulars show the estimated two-dimensional equivalent time of 100 Myr and 140 Myr. Thin line with filled circles (Reference 2D): Parameters except r_H are the same as those of reference case. Thin line with circles (Reference 3D): 3D results corresponding to those of "Reference 2D". Thin dashed line (δT_p=300): δT_p is 300 °C. Other parameters are the same as those of corresponding "Reference 2D". Thick line with filled circles (1/2 Viscosity): η_{ref} is 2.5×10^{20} Pa s. Other parameters are the same as those of corresponding "Reference 2D". Thick dashed line with filled circles (1/2 Viscosity with δT_p=300): δT_p is 300 °C. Other parameters are the same as those of corresponding "1/2 Viscosity". Thin line with large circles (1/2 Velocity): V_s is 5 cm/yr. Other parameters are the same as those of corresponding "Reference 2D".

and 140 Myr, in Fig. 5, since all other calculations are two-dimensional. An example of 3D calculations is shown in Fig. 6.

We expect that the residence time may increase as V_s decreases ("1/2 Velocity"), η_{ref} decreases ("1/2 Viscosity"), and δT_p increases ("δT_p=300" and "1/2 Viscosity with δT_p=300"). Those effects enhance the buoyancy, and thus, the hot anomaly tends to stay longer in the upper mantle. This is true for the cases shown in Fig. 5. However, we also found that the situation is not so simple. Further decrease of viscosity (not shown) decreases the residence time. This occurs because the plume head like hot anomaly becomes thinner because of the interaction of enhanced buoyant hot anomaly with the upper lithosphere. Thus, the maximum temperature becomes low quickly by the combined effects of thinning and heat conduction.

Fig. 7 shows examples of results showing the thermal anomaly over 200 °C about 130 My after the start of calculations.

Fig. 7a is the case with η_{ref} halved and the diameter of thermal anomaly, $2r_H$=3000 km. Fig. 7b shows the same case with the number of finite volumes doubled in each direction and, thus, this result shows the validity of calculations with coarse mesh. We also calculated the temperature-dependent case corresponding to Fig. 9b with doubled resolution and found that the difference is small. For example, the residence times are 142 (coarser resolution) and 141 (finer resolution) Myr.

Although the present dip angle of subducting slab in the NE Honshu is close to 30 degree, the dip angle may change with time. Thus, we look at the effects of

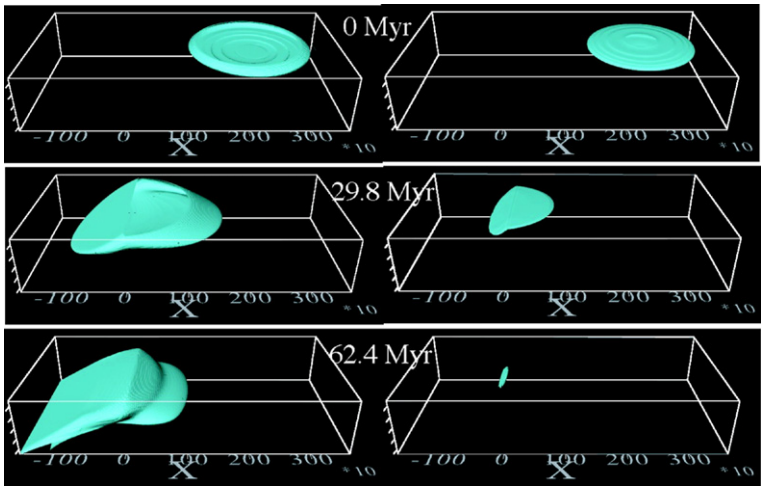

Fig. 6. An example of 3D calculations. The left and right columns show the isotemperature surface of 1301 °C and 1500 °C, respectively. Numerals show the time elapsed after the start of calculations. Note that some part near the top surface cannot be displayed because of software limitations. See Table 2 for the parameters used for this calculation.

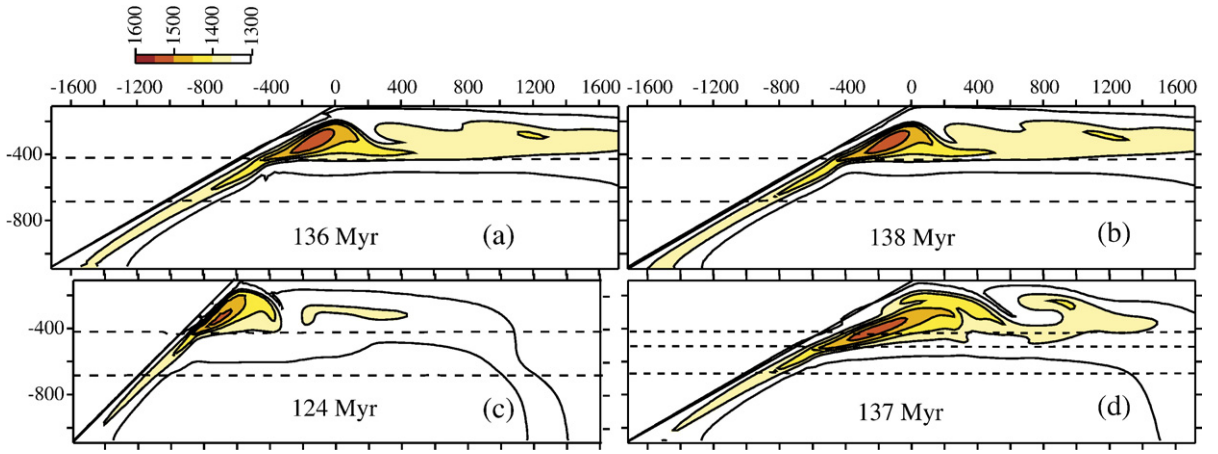

Fig. 7. Results (temperature) of the cases. (a) δT_p=300 °C, $\eta_{ref}=2.5\times10^{20}$ Pa s, r_H=1500 km with 64 finite volumes in the vertical direction. Other parameters are the same as those of reference case, (b) same as (a) with 128 finite volumes in the vertical direction, (c) same as (a) with 45° dip angle and (d) the case with three phase changes. Other parameters are the same as those of (a). For other explanations, see the caption of Fig. 4 and Table 2.

different dip angle (=45°) and the result is shown in Fig. 7c. As one may expect, we found that the residence time decreases (151 Myr for (a) and (b) versus 128 Myr for (c): see Table 2), because the vertical component of the slab velocity increases with steeper dip angle. The shape of thermal anomaly is also controlled by slab angle (however, see next section). This result may provide some general idea on how much ambiguity exist in our results.

A comparison between these results with the tomography shown in Fig. 8 indicates that the high temperature anomaly of our model may be located shallower than the observed low velocity is. This may be adjusted by changing the nature of the phase boundaries. Fig. 7d is the case in which only the physical properties of the phase transitions differ from the case shown in Fig. 7a. We reduced the Clapeyron slope and the density jump at 410 km phase boundary to 2.5 MPa/K and 6%, respectively, and add one more phase boundary at 510 km which may be the wadsleyite–ringwoodite phase transition (Katsura et al., 2004). Its Clapeyron slope and the density jump are set to 6.9 MPa/K (Katsura et al., 2004) and 3%, respectively. We see some penetration of hot anomaly below the 410 km phase boundary which may show a better similarity to the seismic anomaly.

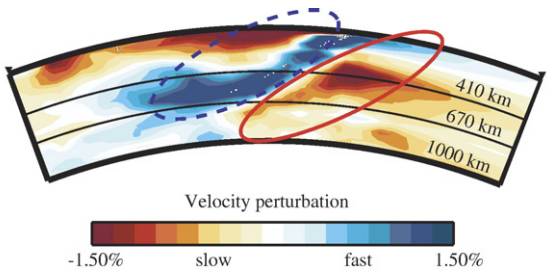

Fig. 8. Closeup of tomographic results by Obayashi et al. (2006). See the caption of Fig. 1 for detail.

3.2. Effects of variable viscosity

Christensen (1984) showed that the non-Newtonian behavior may be mimicked by Newtonian fluid with reduced activation energy (0.3 to 0.5 of the actual activation energy of non-linear creep) for steady state calculation. Although our problem is time-dependent, the flow appears to be rather smooth because of the strong constraints imposed by the plate geometry and speed. Numerically, the Newtonian viscosity is easy to handle and, theoretically, it is easy to scale the problem. Thus, we treat the problem as the Newtonian fluid with reduced activation energy whose magnitude is either 0.3 (153 kJ/mol) or 0.5 (255 kJ/mol) of the activation energy of dislocation creep (510 kJ/mol: Karato and Jung, 2003).

Fig. 9 summarizes the results. Fig. 9a is the case with temperature-independent viscosity and δT_p=325 °C. Fig. 9b shows the case in which the temperature dependent viscosity is taken into account (E=255 kJ/mol) and other parameters are the same as those used in Fig. 9a. The temperature-dependent viscosity helps for the hot anomaly to survive (see Table 2 for the residence times of (a) and (b)). However, the maximum temperature for the case with temperature-dependent viscosity decreases rather quickly at early stage (see the top figures of (a) and (b)). Low viscosity caused by high temperature decreases the drag of plate movement, and, thus, it makes

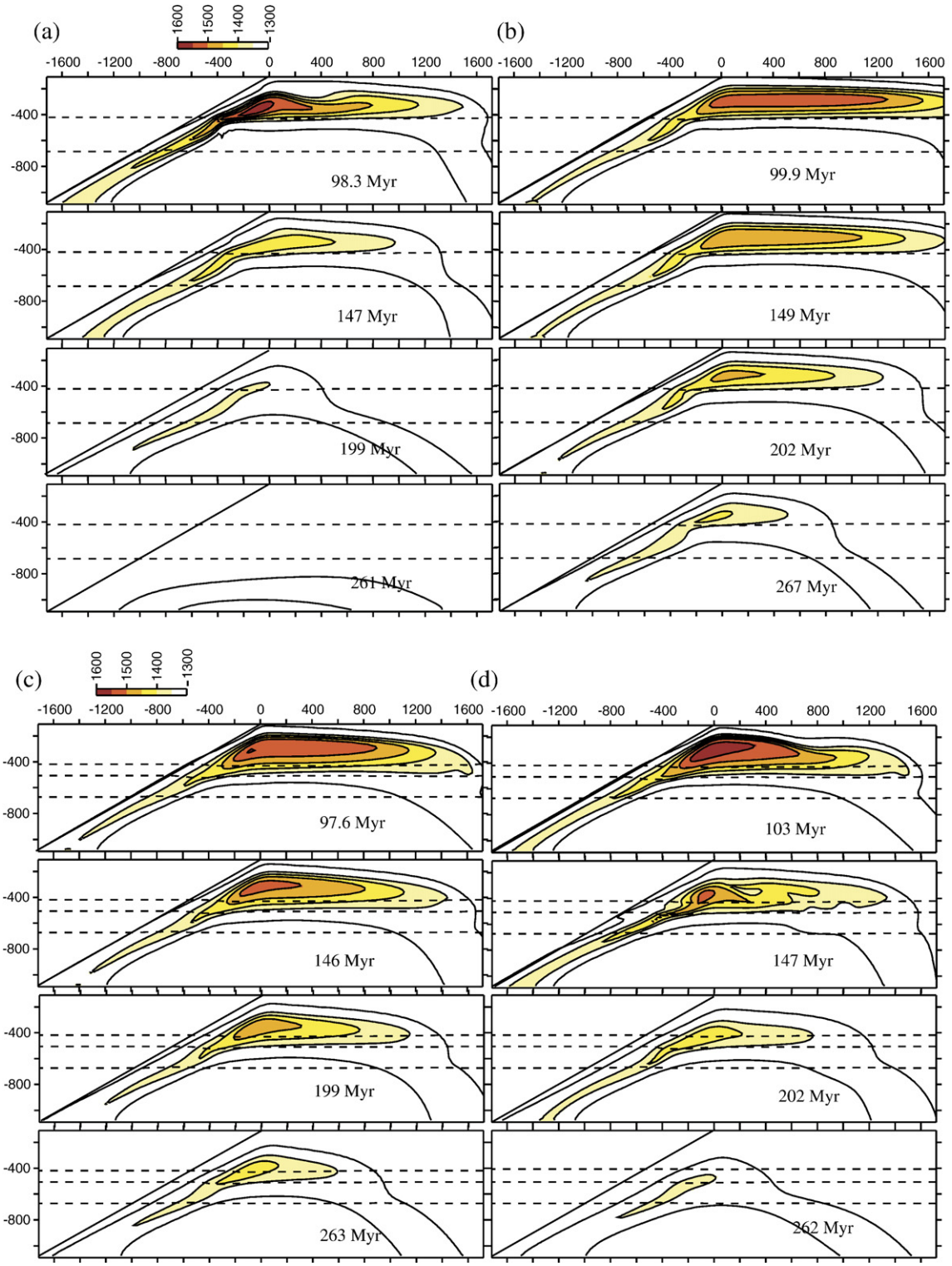

Fig. 9. Results (temperature) showing the effects of temperature-dependent viscosity and the nature of phase changes. δT_p and r_H of all the cases are 325 °C and 1500 km, respectively. (a) Case with temperature-independent viscosity. Except δT_p and r_H, the parameters are the same as those of reference case. (b) Case with temperature-dependent viscosity (E=255 kJ/mol). Other parameters are the same as those of (a). (c) Same as (b) except the nature of phase changes. Three phase changes are included. (d) Same as (c) with weaker temperature dependence of viscosity (E=153 kJ/mol). See Table 2 for more case descriptions.

the residence time longer. On the other hand, the high temperature anomaly will be elongated by the shear caused by the plate movement, and, thus, the maximum temperature drops rather quickly. Note that the tendency of flattening of temperature anomaly before subduction which may be favorable to explain rather flat nature of slow velocity anomaly (Figs. 1 and 8). Fig. 9c and 9d show the cases with three phase boundaries with different activation energy ((c) $E=255$ kJ/mol; (d) $E=153$ kJ/mol), that may make the similarity between the model temperature anomaly and the seismic anomaly better.

4. Conclusions and discussions

We found a close connection between the high temperature anomaly and the 410 km discontinuity in our model. Thus, the model of sinking hot anomaly dragged down by the subducting slab may be more consistent with the observation that shows a good correlation between the slow velocity anomaly and the 410 km discontinuity (Obayashi et al., 2006). However, we also found the deficiency of our simple model, because our results predict rather shallower anomalies than the tomographic result suggests (for example, compare Fig. 8 with Fig. 7a or b). This difficulty may be circumvented by the change of character of the phase change(s) in the transition zone (see Figs. 7d and 9d). Thus, the precise determination of the low velocity zone under the ocean side of the subduction zone may constrain the nature of those phase transitions. This is similar to the situation in which the tomographic results near the 670 km help us to understand the nature of the 670 (660) km seismic discontinuity.

One may suspect that the observation does not appear to support the long entrainment of hot material in our models. We have several explanations. First, the subducting plate of our model moves kinematically even under the 670 km. This is not consistent with the inference that the subducting slab around this region may be stagnant (e.g. Fukao et al., 2001). Also, many dynamical models of subducting slab show such a stagnation, if the slab is weakened (e.g., Tagawa et al., 2007 and references there in). Thus, the actual entrainment may not be so strong as we assumed. Second, possible sporadic movement of sinking slab (e.g., Honda et al., 1993; Tackley et al., 1993) may blur the past trace of entrainment.

By changing the parameters which we think within acceptable ranges as thermal origin of superplume (or plume clusters Schubert et al., 2004), we found that the residence time of hot anomaly staying at the 410 km phase boundary increases over ~100 Myr. Fig. 5 may even suggest an existence of solutions which may be consistent with our scenario based on Kimura et al. (1994) model. Larson (1991a) found the increase of ocean crust formation from 120 to 80 Ma and Tatsumi et al. (1998) estimated the superplume activity from 150 to 90 Ma based on the geochemical analysis of oceanic plateau-related rocks. Our results on the residence time covers these active periods. This might imply a possible link between the past activity of superplume and hot anomaly under the oceanic side of Honshu subduction zone.

One may expect hotspot tracks from the giant hot anomaly, possibly plume head, to the presently active hot spot. However, it is not clear if the hot spot should always appear after the formation of giant plume head. Also, since the plate configuration around the Japanese Islands changes around ~100 Ma (Maruyama et al., 1997), such hot spot tracks might be gone away with presently non-existent plate, i.e., Izanagi-plate (Farrar and Dixon, 1981).

As final discussions, we list other alternative explanations for the slow velocity anomalies: (1) In the high Rayleigh number convection, the hot temperature produced at the upwelling site may extend toward the region near the sinking place. Our model is a modification of this type of phenomena. (2) If the convection is strongly internally heated or it has a strong secular cooling, the highest temperature may be located near the sinking place. (3) A hot anomaly may be created locally by viscous dissipation and/or adiabatic heating. (4) Low velocity zone may be created by the water-related process in the transition zone (Richard et al., 2007). We think that the anomaly produced by processes (2) and (3) are not large enough to explain the Honshu case and may not be correlated with the 410 km discontinuity. The process (4) may be inconsistent with the mainly thermal origin of low velocity zone of our case. In a simple more or less steady convection model, the process (1) may not be prominent enough. It may become prominent, when some sort of event happens as we assumed in this paper. However, we cannot exclude the possibility that the plume(s) may come from the place which is close to the Honshu subduction zone as Obayashi et al. (2006) suggested. Zhao (2004) also pointed out this possibility for his interpretation of slow velocity anomalies beneath the subducting slab based on the arguments given by Malamud and Turcotte (1999). Malamud and Turcotte (1999) proposed the existence of more than 5000 small plumes on the basis of statistical analysis of plume flux and heat budget of the Earth. This may imply that the plumes might come from generally cold region that appears to be somewhat unnatural.

As noted before, the basic underlying questions of this work are: How and where was the hot thermal anomaly created? To solve these questions, it is very important to confirm where this kind of hot anomalies exist. If they exist rather ubiquitously in the subduction zone, we may have to think another mechanisms. From the theoretical point of view, we think that the approach of data assimilation (Ismail–Zadeh et al., 2006) might provide us with some clue to answer these problems, since the forward approach has lots of ambiguities, at least, at present.

Acknowledgement

We thank K. Mibe for his comments in the early stage of this work. P. Tackley suggested us how to make the logic clearer in the earlier version of manuscript. Discussions with Y. Fukao and M. Obayashi were very helpful for understanding seismic tomographic results. M. Obayashi kindly made the base maps of Figs. 1 and 8 for us. Discussions with A. Ismail-Zadeh in lunch and dinner time were very helpful for us to revise the manuscript. Comments by two anonymous reviewers and C. Jaupart greatly improved the original manuscript. The Generic Mapping Tools (Wessel and Smith, 1998) were used in this study. A part of this research was supported by the fund from Ministry of Culture, Sports, Science and Technology and Japan Society for the Promotion of Science.

References

Christensen, U.R., 1984. Convection with pressure- and temperature-dependent non-Newtonian rheology. Geophys. J. R. Astron. Soc. 77, 343–384.

Christensen, U.R., 1996. The influence of trench migration on slab penetration into the lower mantle. Earth Planet. Sci. Lett. 140, 27–39.

Christensen, U.R., Yuen, D.A., 1985. Layered convection induced by phase transitions. J. Geophys. Res. 90, 10291–10300.

Cordery, M.J., Davies, G.F., Campbell, I.H., 1997. Genesis of flood basalts from eclogite-bearing mantle plumes. J. Geophys. Res. 102, 20179–20197.

Farrar, E., Dixon, J.M., 1981. Early Tertiary rupture of the Pacific plate: 1700 km of dextral offset along the Emperor trough–Line Islands. Earth Planet. Sci. Lett. 301–322.

Fukao, Y., Widyantro, S., Obayashi, M., 2001. Stagnant slabs in the upper and lower mantle transition region. Rev. Geophys. 39, 291–323.

Hager, B.H., 1984. Subducted slabs and the geoid: constraints on mantle rheology and flow. J. Geophys. Res. 89, 6003–6016.

Hirose, K., 2002. Phase transitions in pyrolitic mantle around 670-km depth: implications for upwelling of plumes from the lower mantle. J. Geophys. Res. 107, B42078. doi:10.1029/2001JB000597.

Honda, S., Yuen, D.A., Balachandar, S., Reuteler, D., 1993. Three-dimensional instabilities of mantle convection with multiple phase transitions. Science 259, 1308–1311.

Ismail-Zadeh, A., Schubert, G., Tsepelev, I., Korotkii, A., 2006. Three-dimensional forward and backward numerical modeling of mantle plume evolution: effects of thermal diffusion. J. Geophys. Res. 111, B06401. doi:10.1029/2005JB003728.

Kárason, H., van der Hilst, R.D., 2000. Constraints on mantle convection from seismic tomography. The History and Dynamics of Global Plate Motion. . Geophys. Monogr., vol. 121. Amer. Geophys. Uni., Washington, pp. 277–288.

Karato, S., Jung, H., 2003. Effects of pressure on high-temperature dislocation in olivine. Philo. Mag. 83, 401–414.

Katsura, T., Yamada, H., Nishikawa, O., Song, M., Kubo, A., Shinmei, T., Yokoshi, S., Aizawa, Y., Yoshino, T., Walter, M., Ito, E., 2004. Olivine–wadsleyite transition in the system $(Mg,Fe)_2$ SiO_4. J. Geophys. Res. 109, B02209. doi:10.1029/2003JB002438.

Kimura, G., Sakakibara, M., Okamura, M., 1994. Plumes in central Panthalassa? Deductions from accreted oceanic fragments in Japan. Tectonics 13, 905–916.

Lambeck, K., Johnston, P., 1998. The viscosity of the mantle: evidence from analysis of glacial rebound phenomena. In: Jackson, I. (Ed.), The Earth's Mantle, Composition, Structure, and Evolution. Cambridge Univ. Press, pp. 461–502.

Larson, R.L., 1991a. Latest pulse of Earth: evidence for a mid-Cretaceous superplume. Geology 19, 547–550.

Larson, R.L., 1991b. Geological consequences of superplumes. Geology 19, 963–966.

Malamud, B.D., Turcotte, D.L., 1999. How many plumes are there? Earth Planet. Sci. Lett. 174, 113–124.

Maruyama, S., Isozaki, Y., Kimura, G., Terabayashi, M., 1997. Paleogeographic maps of the Japanese Islands: plate tectonic synthesis from 750 Ma to the present. The Island Arc 6, 121–142.

Miller, M.S., Kennett, B.L.N., Gorbatov, A., 2006. Morphology of the distorted subducted Pacific slab beneath the Hokkaido corner, Japan. Phys. Earth Planet. Inter. 156, 1–11.

Obayashi, M., Sakurai, T. Fukao, Y., 1997. Comparison of recent tomographic models (abstract). in: Suyehiro, K. (ed.), International Symposium on New Images of the Earth's Interior Through Long-Term Ocean-Floor Observations. Earthquake Research Institute, Univ. of Tokyo, pp 29.

Obayashi, M., Sugioka, H., Yoshimitsu, J., Fukao, Y., 2006. High temperature anomalies oceanward of subducting slabs at the 410-km discontinuity. Earth Planet. Sci. Lett. 243, 149–158.

Piomallo, C., Moreili, A., 2003. P wave tomography of the mantle under the Alpine–Mediterranean area. J. Geophys. Res. 108, 2065. doi:10.1029/2021JB001757.

Richard, G., Monnereau, M., Rabinowicz, M., 2007. Slab dehydration and fluid migration at the base of the upper mantle: implications for deep earthquake mechanisms. Geophys. J. Int. 168, 1291–1304.

Schubert, G., Yuen, D.A., Turcotte, D.L., 1975. Role of phase transition in a dynamical mantle. Geophys. J. R. Astron. Soc. 42, 441–460.

Schubert, G., Masters, G., Olson, P., Tackley, P., 2004. Superplumes or plume clusters? Earth Planet. Sci. Lett. 146, 147–162.

Tackley, P.J., 1993. Effects of strongly temperature-dependent viscosity on time-dependent, three-dimensional models of mantle convection. Geophys. Res. Lett. 20, 2187–2190.

Tackley, P.J., Stevenson, D.J., Glatzmaier, G.A., Schubert, G., 1993. Effects of an endothermic phase transition at 670 km depth on spherical mantle convection. Nature 361, 699–704.

Tagawa, M., Nakakuki, T., Tajima, F., 2007. Dynamical modeling of trench retreat driven by the slab interaction with the mantle transition zone. Earth Planets Space 59, 65–74.

Tatsumi, Y., Shinjoe, H., Ishizuka, H., Sager, W., Klaus, A., 1998. Geochemical evidence for a mid-Cretaceous superplume. Geology 26, 151–154.

Terabayashi, M., Okamoto, K., Yamamoto, H., Kaneko, Y., Ota, T., Maruyama, S., Katayama, I., Komiya, T., Ishikawa, A., Anma, R., Ozawa, H., Windley, B., Liou, J.G., 2005. Accretionary complex origin of the mafic–ultramafic bodies of the Sanbagawa belt, Central Shikoku, Japan. Int. Geol. Rev. 47, 1058–1073.

Ueda, H., 2005. Accretion and exhumation structures formed by deeply subducted seamounts in the Kamuikotan high-pressure/temperature zone, Hokkaido, Japan. Tectonics 24. doi:10.1029/2004TC001690.

van der Hilst, R.D., Widiyantoro, S., Engdahl, E.R., 1997. Evidence for deep mantle circulation from global tomography. Nature 386, 578–584.

van Hunen, J., van den Berg, A., Vlaar, N., 2001. Latent heat effects of major mantle phase transitions on low-angle subduction. Earth Planet. Sci. Lett. 190, 125–135.

VanDecar, J., James, D., Assumpcao, M., 1995. Seismic evidence for a fossil mantle plume beneath South America and implications for plate driving forces. Nature 378, 25–31.

Wessel, P., Smith, W.H.F., 1998. New improved version of the Generic Mapping Tools released. EOS, Trans. Am. Geophys. Union 79 (47), 579.

Widiyantoro, S., 1997. Studies of seismic tomography on regional and global scale, Ph. D. thesis, Aust. Natl. Univ. Canberra, A.C.T., Australia.

Zhao, D., 2004. Global tomographic images of mantle plumes and subducting slabs: insight into deep Earth dynamics. Phys. Earth Planet. Inter. 146, 3–34.

Zhao, D., Xu, Y., Wiens, D.A., Dorman, L., Hildebrand, J., Webb, S., 1997. Depth extent of the Lau back-arc spreading center and its relation to subduction processes. Science 278, 254–257.

Zhong, S., Gurnis, M., 1994. Role of plates and temperature-dependent viscosity in phase change dynamics. J. Geophys. Res. 99, 15903–15918.